Chaos, Solitons and Fractals 167 (2023) 112992

Contents lists available at ScienceDirect

Chaos, Solitons and Fractals

journal homepage: www.elsevier.com/locate/chaos

Symbolic convergent cross mapping based on permutation mutual information

Xinlei Ge, Aijing Lin *

School of Mathematics and Statistics, Beijing Jiaotong University, Beijing 100044, PR China

ARTICLE INFO

Keywords:
Causality analysis
Convergent cross mapping
Permutation mutual information
Physiological system

ABSTRACT

In this paper, we extend convergent cross mapping (CCM) and propose symbolic CCM (SCCM), which uses mutual information based on permutation pattern instead of Pearson correlation coefficient to estimate cross-mapping ability. We numerically demonstrate that SCCM is a robust method for quantifying information flow between time series in chaotic systems, even under the influence of noises. Using the method, we analyze the multichannel EEG signals of ADHD children and control children, and identify the differences between the two groups of subjects with reliable results.

1. Introduction

The study of complex systems requires modeling for multidimensional signals [1]. Discovering relationships among signals is also essential for research. A prominent example of physiological system is the establishment that the interactive structure of brain network is closely related to a range of physiological states [2,3]. With the rapid growth of observational and simulated data, many data-driven causal inference methods under different frameworks have been proposed [4–7], which show great improvements over (Pearson) correlation and regression methods [8].

Convergent cross mapping (CCM) as a causal measure method based on phase space reconstruction was originally used to detect causality in weakly coupled ecosystems [7] and gradually attracted many scholars to improve it and apply it to more kinds of systems [9–19]. Sugihara et al. [7] derived the definition of cross-mapping ability by quantifying how accurately the cause variable X can be estimated from historical information on the result variable Y. Simply put, the cross-mapping ability is the Pearson correlation coefficient between the estimated value and the true value of variable X. As the data length increases, if there is indeed a causal relationship, the effective information will gradually increase, so the cross-mapping ability also converges to the maximum value. Thus the convergence of cross-mapping ability is an important indicator for CCM to distinguish correlation from causality.

One disadvantage of CCM is its sensitivity to noise. Since the coupling between real data is often a mixture of stochastic oscillations and deterministic mechanisms [10], improving the reliability of the algorithm is also one of the research hotspots. Mønster et al. [16] proposed that adding noises in a medium-strong coupling system can achieve more accurate causal inference when taking advantage of the characteristic that the convergence rate is not sensitive to noise. Compared with the improvement in Ref. [16] which focuses on the cross-mapping step, Feng et al. [17] proposed to use a Gaussian processes to improve the phase space reconstruction technique, thereby constructing a more stable attractor manifold to achieve robustness against noise. Supported by the theory of symbolic dynamics, Stavroglou et al. [18,19] redefined cross-mapping ability by using pattern causality instead of the Pearson correlation coefficient.

For nonlinear systems, symbolic method based on permutation pattern defines symbols by comparison of neighboring values and thus reduces the sensitivity to noise more effectively [20]. Such advantages also facilitate the use of symbolic techniques to investigate the intrinsic ordinal structures in complex systems. Staniek and Lehnertz [21] proposed symbolic transfer entropy, which reliably identifies the location of epileptic focus without observing actual seizure activity. Furthermore, many dissimilarity measure methods based on permutation pattern have been developed to analyze physiological signals [22–24].

In this paper, we extend CCM and propose symbolic CCM (SCCM), which uses mutual information based on permutation pattern instead of Pearson correlation coefficient to estimate cross-mapping ability. The main contribution of this paper is to introduce permutation pattern into CCM from symbolic dynamics perspective, which can effectively eliminate the impact of stochastic noises. First, we verify that SCCM has the same robustness as CCM through two classical chaotic models. Then, we analyze simulated experiments masked with white Gaussian noise and find that SCCM has stronger noise immunity than CCM.

* Corresponding author.
E-mail addresses: gexinlei@bjtu.edu.cn (X. Ge), ajlin@bjtu.edu.cn (A. Lin).

https://doi.org/10.1016/j.chaos.2022.112992
Received 3 October 2022; Received in revised form 15 November 2022; Accepted 4 December 2022
Available online 20 December 2022

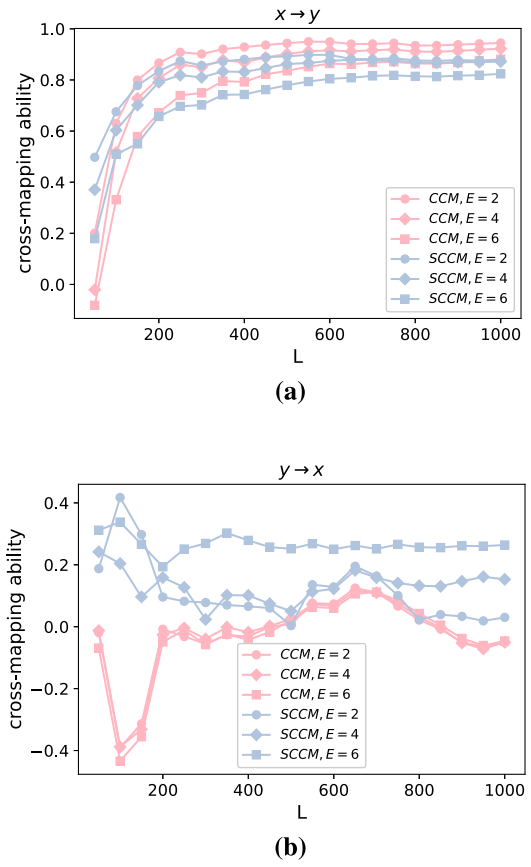

Fig. 1. The cross-mapping ability for CCM and SCCM as a function of time series length L in simulation 1. (a) x causes y. (b) y causes x.

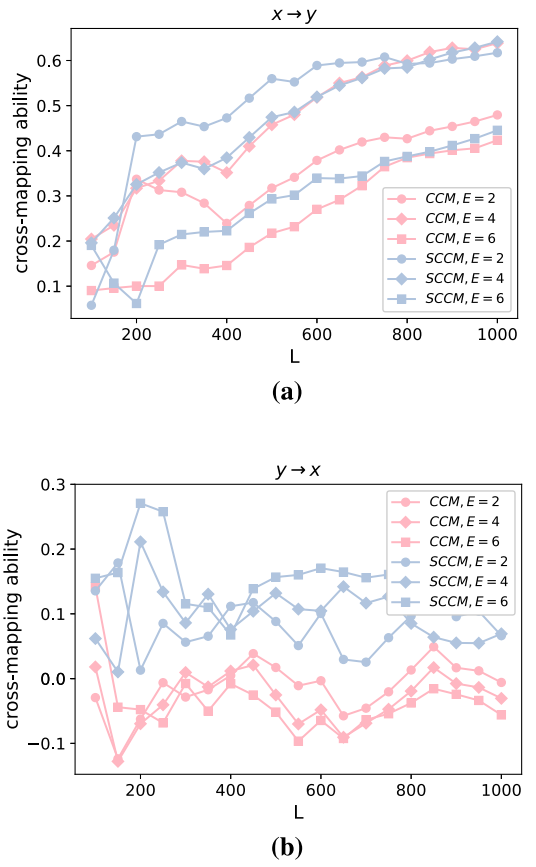

Fig. 2. The cross-mapping ability for CCM and SCCM as a function of time series length L in simulation 2. (a) x causes y. (b) y causes x.

Finally, based on EEG signals collected from children with attention deficit hyperactivity disorder (ADHD) and control children, we analyze both from a network perspective and specific numerical outcomes to complement and deepen the understanding of causal relationships in physiological systems. Compared with CCM, which is easily affected by systematic bias and will lead to miscalculation of ADHD subjects, the results of SCCM in all areas show that there are significant and stable differences between the two groups of subjects, especially in the anterior area. This method also provides some reference for disease diagnosis.

The structure of this paper is as follows. Section 2 presents the methods employed in this study. Section 3 describes the data and analyzes the obtained results. Section 4 gives the conclusions.

2. Methods

2.1. Permutation mutual information

Inspired by permutation entropy (PE) [20] and mutual information (MI) [25], Yin et al. [26] proposed permutation mutual information (PMI) to study the mutual information based on permutation pattern. In this section, we first briefly review the PE, and then introduce the calculation of PMI.

Taking time series $\{x_t\}_{t=1}^{T}$ as an example, we construct its time-delay embedding vectors $X_t^{m,\tau} = [x_t, x_{t+\tau}, x_{t+2\tau}, \dots, x_{t+(m-1)\tau}]$ for $t = 1, 2, \dots, T-(m-1)\tau$, where m and τ denote the embedding dimension and time delay, respectively. For each time t, $X_t^{m,\tau}$ can be mapped to a permutation pattern $\pi_l^{m,\tau}$ for $i = 1, 2, \dots, m!$ (representing all unique orderings of different numbers). In our paradigm, taking $E = 3$ as an example, there are 3! patterns: π_1: (012) means $x_t < x_{t+\tau} < x_{t+2\tau}$, π_2: (021) means $x_t < x_{t+2\tau} < x_{t+\tau}$, π_3: (102) means $x_{t+\tau} < x_t < x_{t+2\tau}$, π_4: (120) means $x_{t+\tau} < x_{t+2\tau} < x_t$, π_5: (201) means $x_{t+2\tau} < x_t < x_{t+\tau}$ and π_6: (210) means $x_{t+2\tau} < x_{t+\tau} < x_t$. For each π, we determine the relative frequency

$$p\left(\pi_l^{m,\tau}\right) = \frac{\left\|\left\{k : k \le T, \text{type}\left(X_k^{m,\tau}\right) = \pi_l^{m,\tau}\right\}\right\|}{T} \tag{1}$$

where $type(\cdot)$ denotes the map from time-delay embedding vector to permutation pattern and $\|\cdot\|$ denotes the cardinality of a set. Thus, PE is defined as the Shannon entropy of the $m!$ distinct symbols:

$$H(x, m, \tau) = -\sum_{l=1}^{m!} p\left(\pi_l^{m,\tau}\right) \log p\left(\pi_l^{m,\tau}\right). \tag{2}$$

With the view of two time series $\{x_t\}_{t=1}^{T}$ and $\{y_t\}_{t=1}^{T}$, permutation mutual information is proposed by replacing Shannon entropy with mutual information. The process is the same as PE, and the first step is to construct their time-delay embedding vectors $\{X_t^{m,\tau}\}$ and $\{Y_t^{m,\tau}\}$. Thus, $p\left(\pi_l^{m,\tau}\right)$ for $\{x_t\}_{t=1}^{T}$ and $\{y_t\}_{t=1}^{T}$ can be respectively denoted as:

$$p_x\left(\pi_l^{m,\tau}\right) = \frac{\left\|\left\{k : k \le T, type\left(X_k^{m,\tau}\right) = \pi_l^{m,\tau}\right\}\right\|}{T}, \tag{3}$$

$$p_y\left(\pi_l^{m,\tau}\right) = \frac{\left\|\left\{k : k \le T, type\left(Y_k^{m,\tau}\right) = \pi_l^{m,\tau}\right\}\right\|}{T}. \tag{4}$$

The joint probability $p_{xy}\left(\pi_i^{m,\tau}, \pi_j^{m,\tau}\right)$ can also be calculated as:

$$p_{xy}\left(\pi_i^{m,\tau}, \pi_j^{m,\tau}\right) = \frac{\left\|\left\{k : k \le T, type\left(X_k^{m,\tau}, Y_k^{m,\tau}\right) = \left(\pi_i^{m,\tau}, \pi_j^{m,\tau}\right)\right\}\right\|}{T}. \tag{5}$$

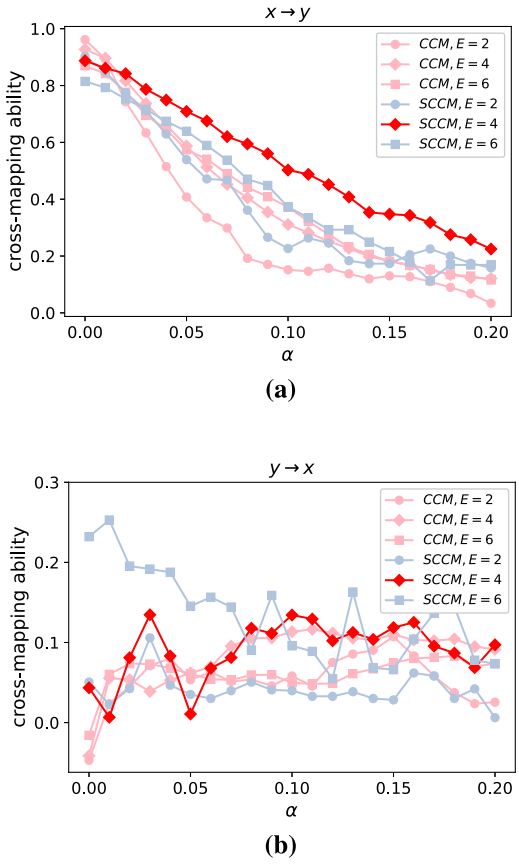

Fig. 3. The cross-mapping ability for CCM and SCCM as a function of noise strength α in simulation 1 masked with white Gaussian noise. (a) x causes y. (b) y causes x.

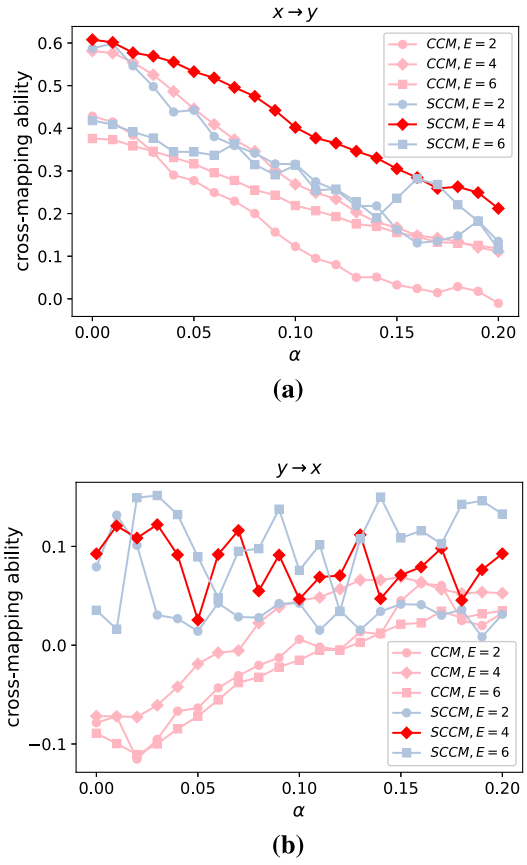

Fig. 4. The cross-mapping ability for CCM and SCCM as a function of noise strength α in simulation 2 masked with white Gaussian noise. (a) x causes y. (b) y causes x.

Then, PMI can be defined based on the above probability distribution as:

$$\begin{aligned} PMI(x,y,m,\tau) &= H(x,m,\tau) + H(y,m,\tau) - H(x,y,m,\tau) \\ &= -\sum_{l=1}^{m!} p_x\left(\pi_l^{m,\tau}\right)\log p_x\left(\pi_l^{m,\tau}\right) - \sum_{l=1}^{m!} p_y\left(\pi_l^{m,\tau}\right)\log p_y\left(\pi_l^{m,\tau}\right) \\ &+ \sum_{i=1}^{m!}\sum_{j=1}^{m!} p_{xy}\left(\pi_i^{m,\tau},\pi_j^{m,\tau}\right)\log p_{xy}\left(\pi_i^{m,\tau},\pi_j^{m,\tau}\right). \end{aligned} \tag{6}$$

When dimension m is larger, PMI will show a false larger value. In order to eliminate this effect, the adjusted measure [27] for PMI may then be defined to be:

$$\begin{aligned} &APMI(x,y,m,\tau) \\ &= \frac{PMI(x,y,m,\tau) - E\{PMI(x,y,m,\tau)\}}{1/2\{H(x,m,\tau) + H(y,m,\tau)\} - E\{PMI(x,y,m,\tau)\}}, \end{aligned} \tag{7}$$

where $E\{PMI(x,y,m,\tau)\}$ is the expected PMI between x and y.

Under the assumption of Gaussian distribution, MI can be expressed as [28,29]:

$$MI(x,y) = -\frac{1}{2}log(1-r^2), \tag{8}$$

where r denotes the coefficient of correlation between x and y. For better comparison with the correlation coefficient, it is natural to define a measure named Gaussian APMI (GAPMI):

$$GAPMI(x,y,m,\tau) = \sqrt{1-\exp^{-2APMI(x,y,m,\tau)}}. \tag{9}$$

2.2. Convergent cross mapping

Convergent cross mapping (CCM) is to identify causality between time series that are from the same dynamic system. Consider two time series $\{x_t\}_{t=1}^{T}$ and $\{y_t\}_{t=1}^{T}$. The specific process to measure causality from x to y is as follows:

Step1: Similar to Section 2.1, we reconstruct the system by forming the time-delay embedding vectors $X_t^{m,\tau}$ and $Y_t^{m,\tau}$ for $t = 1,2,\ldots,T-(m-1)\tau$, where these set of vectors are called the reconstruction manifold $\boldsymbol{M}_X$ and $\boldsymbol{M}_Y$, respectively.

Step2: Given a point $Y_t^{m,\tau}$ in $\boldsymbol{M}_X$, we find its $E+1$ nearest neighbors and order the time indices (from closest to farthest) by $t_1, t_2, \ldots, t_{E+1}$. These corresponding time indices are applied to identifying nearby points in $\boldsymbol{M}_X$.

Step3: x_t is estimated from a locally weighted mean of the $E+1$ x_{t_i} values.

$$\hat{x}_t \mid \boldsymbol{M}_Y = \sum_{i=1}^{E+1} w_i x_{t_i} \tag{10}$$

where w_i is a weighting based on the distance between $Y_t^{m,\tau}$ and its ith nearest neighbor $Y_{t_i}^{m,\tau}$ on $\boldsymbol{M}_Y$. The weights are determined by

$$w_i = u_i / \sum_{j=1}^{E+1} u_j \tag{11}$$

where

$$u_i = \exp\left\{-d\left[Y_t^{m,\tau}, Y_{t_i}^{m,\tau}\right] / d\left[Y_t^{m,\tau}, Y_{t_1}^{m,\tau}\right]\right\} \tag{12}$$

and $d[Y_s, Y_t]$ is the Euclidean distance between two vectors.

Step4: We repeat steps 2–3 for every point in $\boldsymbol{M}_X$ and calculate the cross mapping coefficients $CCM_{X\to Y}$ by Pearson correlation between observed and predicted values.

$$CCM_{X\to Y} = \frac{\sum(x_t - \bar{x}_t)(\hat{x}_t - \bar{\hat{x}}_t)}{\sqrt{\sum(x_t - \bar{x}_t)^2 \sum(\hat{x}_t - \bar{\hat{x}}_t)^2}} \tag{13}$$

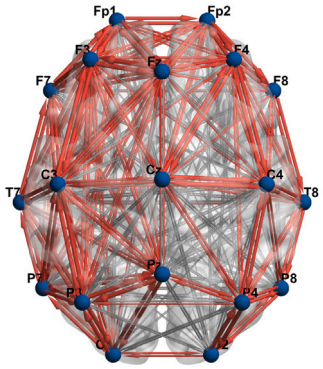

(a)

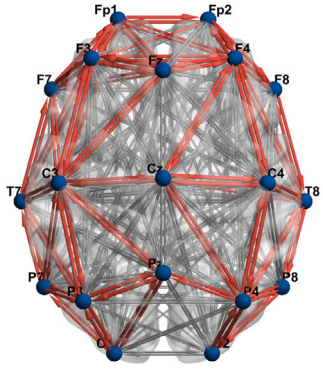

(b)

Fig. 5. Interactive information flow of brain network based on the mean CCM value. The red directional arrow represents the values greater than 0.5; otherwise they are gray. (a) Control subjects. (b) ADHD subjects.

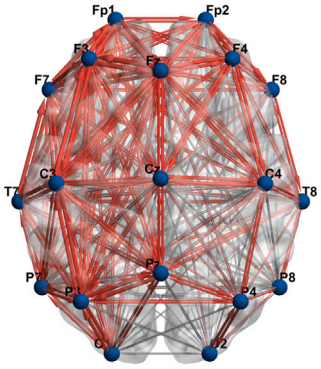

(a)

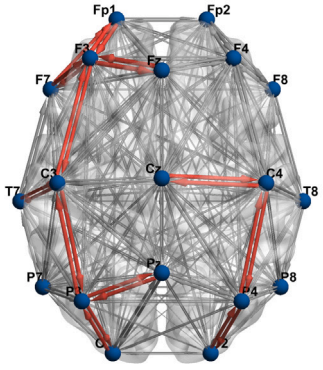

(b)

Fig. 6. Interactive information flow of brain network based on the mean SCCM value. The red directional arrow represents the values greater than 0.35; otherwise they are gray. (a) Control subjects. (b) ADHD subjects.

2.3. Symbolic CCM based on PMI

Steps 1 and 2 are the same as CCM method.

Step3: Different from CCM, which directly estimates the value of time series $\hat{x}_t$, SCCM estimates the average pattern $\hat{S}_t^x$ through the given $E+1$ time indices.

$$\hat{S}_t^x = type\left(\hat{X}_t^{m,\tau} \mid \boldsymbol{M}_{\boldsymbol{Y}}\right), \tag{14}$$

where $type(\cdot)$ denotes the map from time-delay embedding vector to permutation pattern and

$$\hat{X}_t^{m,\tau} \mid \boldsymbol{M}_{\boldsymbol{Y}} = \sum_{i=1}^{E+1} w_i \hat{X}_{t_i}^{m,\tau}, \tag{15}$$

w_i is the same defined weight as CCM. Similarly, the real pattern S_t^x can also be defined as

$$S_t^x = type\left(X_t^{m,\tau}\right). \tag{16}$$

Step4: In the same way, we compute the estimated patterns and real patterns corresponding to all points. Thus, $p\left(\pi_l^{m,\tau}\right)$ for $\hat{S}^x$, S^x and their joint probability can be respectively denoted as:

$$p_{\hat{S}}\left(\pi_l^{m,\tau}\right) = \frac{\left\|\left\{k : \hat{S}_k^x = \pi_l^{m,\tau}\right\}\right\|}{len(\hat{S}^x)}, \tag{17}$$

$$p_S\left(\pi_l^{m,\tau}\right) = \frac{\left\|\left\{k : S_k^x = \pi_l^{m,\tau}\right\}\right\|}{len(S^x)}, \tag{18}$$

$$p_{\hat{S}S}\left(\pi_i^{m,\tau}, \pi_j^{m,\tau}\right) = \frac{\left\|\left\{k : \left(\hat{S}_k^x, S_k^x\right) = \left(\pi_i^{m,\tau}, \pi_j^{m,\tau}\right)\right\}\right\|}{len(S^x)}, \tag{19}$$

where $len(\cdot)$ denotes the length of time series. Finally, the GAPMI between the estimated patterns and real patterns is calculated and defined as $SCCM_{X\to Y}$.

$$SCCM_{X\to Y} = GAPMI(\hat{S}_t^x, S_t^x, m, \tau). \tag{20}$$

In the next section, we will discuss the effect of embedded dimension on the results, but not the time delay. Because compared with E, the calculation amount caused by the change of τ is much less. Usually, $\tau = 1$ is suitable for the models in this paper without over sampling.

3. Simulation experiments

3.1. Simulation experiments on chaotic model

To demonstrate that SCCM can provide the same reliable results as CCM, we adopt two classical chaotic models, which are nonlinear, non-periodic and deterministic.

The first numerical example is a coupled two-species nonlinear logistic difference system with constant coefficients that exhibit chaotic behavior [7]. The equations are expressed as follows:

$$\begin{aligned} x_{t+1} &= x_t(r_x - r_x x_t - \beta_{yx} y_t), \\ y_{t+1} &= y_t(r_y - r_y y_t - \beta_{xy} x_t), \end{aligned} \tag{21}$$

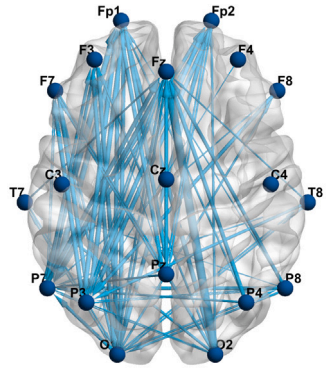

(a)

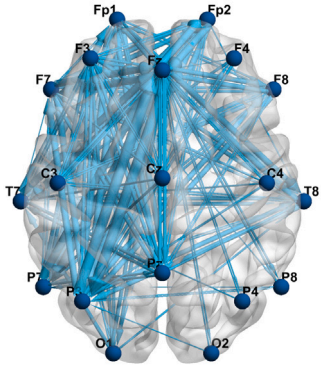

(b)

Fig. 7. Interactive information flow of brain network based on the absolute differences between ADHD subjects and Control subjects. The blue directional arrow represents values greater than 0.1. (a) CCM. (b) SCCM. (For interpretation of the references to color in this figure legend, the reader is referred to the web version of this article.)

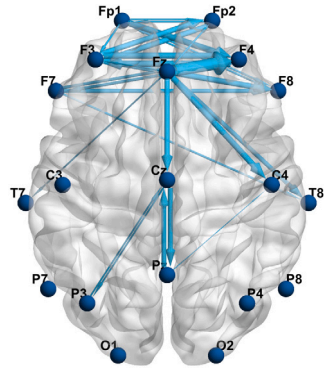

Fig. 8. Interactive information flow of brain network based on the absolute differences between Figs. 7(a) and 7(b). The blue directional arrow represents values greater than 0.1. (For interpretation of the references to color in this figure legend, the reader is referred to the web version of this article.)

where $r_x = 3.8$, $r_y = 3.5$, β represents the coupling strength and starting conditions $x_1 = 0.2$, $y_1 = 0.3$.

Another numerical example is unidirectionally coupled Henon maps model [30],

$$\begin{aligned} x_t &= 1.4 - x_{t-1}^2 + 0.3x_{t-2}, \\ y_t &= 1.4 - (Cx_{t-1} + (1-C)y_{t-1})y_{t-1} + 0.3y_{t-2}, \end{aligned} \tag{22}$$

where C represents the coupling strength and starting conditions $x_0 = (0.1, 0.3)$, $y_0 = (0.1, 0.3)$.

In our experiments, we only consider unidirectional coupling from x to y, that is, $\beta_{yx} = 0, \beta_{xy} = 0.1$ in Eqs. (21) and $C = 0.2$ in Eqs. (22). We intercepted fragments of different lengths to calculate CCM and SCCM under different embedded dimension E respectively. Figs. 1–2 shows the simulation results. From the results of x to y, SCCM is similar to CCM and shows the convergence property, so it can correctly identify causality between time series. Compared with simulation 1 in Fig. 1(a), the results of simulation 2 in Fig. 2(a) are more susceptible to the embedded dimension E. CCM and SCCM both have quite good accuracy of cross-mapping when $E = 4$. On the contrary, when there is no causal relationship (see Figs. 1(b) and 2(b)), all results remain at a relatively low level. Through the above experiments, we can also find that when the data length is 1000, both CCM and SCCM can obtain stable results. So, in subsequent experiments, we set all the data lengths to 1000.

To further compare the difference between CCM and SCCM under the influence of observation noise, we add white Gaussian noise to simulation 1 and simulation 2. The equations are expressed as follows:

$$\begin{aligned} x_t' &= x_t^* + \alpha\varepsilon_{x,t}, \\ y_t' &= y_t^* + \alpha\varepsilon_{y,t}, \end{aligned} \tag{23}$$

where x_t^* and y_t^* represent the normalized x_t and y_t, $\varepsilon_t \sim N(0,1)$, and α represents noise strength.

As can be seen from Figs. 3(b) and 4(b), for directions without causality, the effects of noise strength on the results are not significantly different. But as illustrated in Figs. 3(a) and 4(a), the results in the opposite directions happen to be completely different. The cross-mapping ability gradually decreases with the increase of noise strength α. It is worth noting that the effect of noise on the results of different embedding dimensions and different methods is also different. Permutation pattern can effectively reduce the sensitivity to noise. In other words, under the same conditions, SCCM is more stable than CCM. Nevertheless, the two methods show some similarities. The robustness is strongest at the optimal E, such as in simulation 2. When the optimal E is uncertain, or when the noise-free results for different E are similar, the smaller E is, the worse the robustness is, as in simulation 1. In both simulations, SCCM shows the best performance at $E = 4$. The difference is that SCCM shows the best performance in simulation 1 at $E = 4$, which indicates that a too high dimension E will also produce SCCM calculation error to a certain extent.

3.2. Simulation experiments on multichannel EEG signals

The subjects of EEG signals are 61 ADHD children and 60 control children [31,32]. During the experiment, 19 electrode channel signals (Fz, Cz, Pz, C3, T3, C4, T4, Fp1, Fp2, F3, F4, F7, F8, P3, P4, T5, T6, O1, O2) on the scalp are recorded at a sampling frequency of 128 Hz based on the 10–20 system. The original sample data are obtained from IEEE Data Port (https://ieee-dataport.org/open-access/eeg-data-adhd-control-children). Here, we use the BrainNet Viewer (http://www.nitrc.org/projects/bnv/) to visualize the results [33], as shown in Figs. 5–8.

Considering that the experimental time of each child is inconsistent, we use a sliding window with a length of 1000 to record the time-varying interaction information between channels. Then, the average value of each window calculation result is taken to represent the result of the whole signal. After the above processing, the influence of selecting an abnormal segment on the result can also be avoided, thereby making the results more accurate and effective.

We start comparing CCM and SCCM from the perspective of information flow networks. Figs. 5 and 6 display the mean CCM and SCCM values between all pairs of EEG channels. Red arrows indicate that the values are greater than the threshold; otherwise they are gray. In both experiments, we can draw the same conclusion that the control subjects show more information flow than the ADHD subjects. Relatively speaking, the left area of the control subjects is more active.

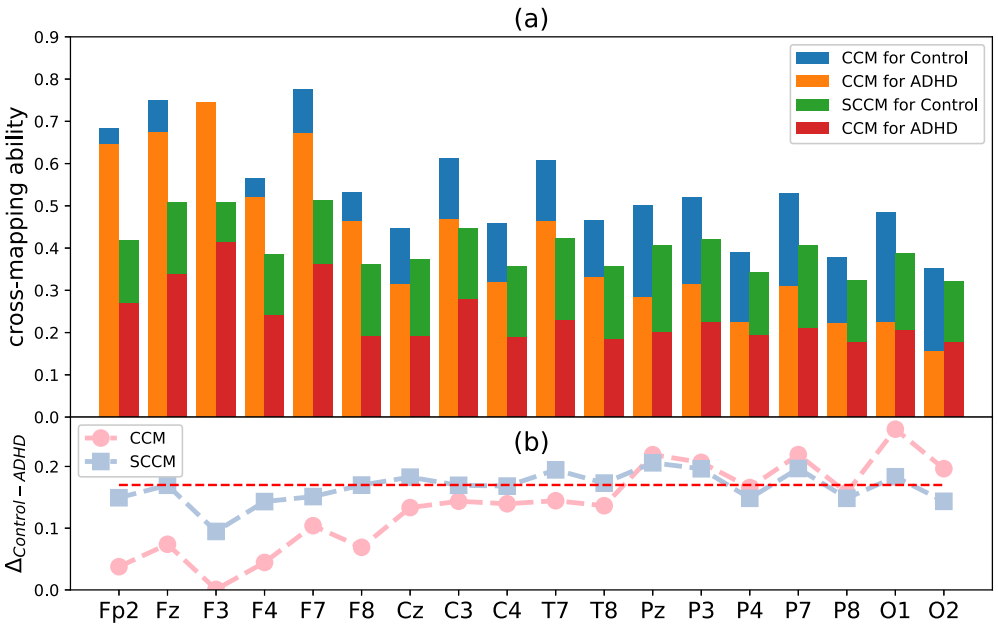

Fig. 9. (a) The results of the effect of Fp1 as a driving variable on the other channels. (b) The differences between ADHD subjects and Control subjects based on (a).

The difference is that the overall results of the CCM calculations are all skewed larger than those of the SCCM. We speculate that the signals are susceptible to the same noise during collection, such as interference from recording instruments or other brain activity, leading to some synchronized behavior. Next, we compute the absolute differences between the mean values of ADHD subjects and control subjects, as shown in Fig. 7. In order to further compare CCM and SCCM, we continue to calculate the absolute differences between the results in Figs. 7(a) and 7(b), and the results are shown in Fig. 8. According to Fig. 8, the difference between the results of the two methods is mainly in the anterior area (Fp1, Fp2, F7, F3, Fz, F4, F8). By CCM, ADHD subjects and control subjects do not have significantly different information flow in this area. In contrast, SCCM can effectively distinguish ADHD subjects from control subjects by the change in information flow in this area.

Then, the channel Fp1 is used as an example to explore the interaction with other channels by specific numerical results. Fig. 9a shows the results of the effect of Fp1 as a driving variable on the other channels. Obviously, the spatial location of the channels directly affects the degree of information interaction. Fp1 has a stronger causal effect on the channels that are in adjacent areas; in other words, a greater effect on the left and anterior area than on the right and posterior area. Similar to the previous procedure, we calculate the differences between ADHD and control subjects for each method separately. Fig. 9b shows the same results as Fig. 8, with a relatively insignificant discrepancy in the numerical results of CCM in the anterior area for both types of subjects. In terms of this result, we can speculate that systematic deviations will lead to the misjudgment of the ADHD subjects. Compared with CCM, the results of SCCM in all areas indicate significant and stable discrepancy of the two groups of subjects especially in the anterior area. In the previous part, we focus on the mean results of the subjects. Next, we pick three typical channel pairs (Fp1→Fz, Fp1→Pz, Fp1→O1) from Fig. 9 and represent the results for specific subjects through box plots. It can be found from Fig. 10 that the distance between the channels significantly affects the performance of CCM in distinguishing ADHD subjects and control subjects. The signals between adjacent channels are easily affected by the same noises, resulting in no significant difference in the results of CCM method on the two types of subjects. For the case of Fp1→O1, the CCM and SCCM results are similar because the distance is sufficient to minimize the effect of noise. Pz is located in the middle of brain, and the results of two groups calculated by CCM also show an incompletely differentiated state. It is worth mentioning that SCCM achieves the expected results in all cases, providing a certain reference for disease diagnosis.

4. Conclusion

In this paper, we propose symbolic convergent cross mapping based on permutation mutual information for chaotic systems. The simulation results for both artificial and real-world datasets show the validity of our method. Our method facilitates detailed understanding of the interactive information structure of physiological systems under observational noises, which in turn aids in the diagnosis of diseases. In the future, we expect our proposed method will be popularized in more fields.

CRediT authorship contribution statement

Xinlei Ge: Conceptualization, Methodology, Software, Validation, Formal analysis, Investigation, Data curation, Writing – original draft. **Aijing Lin:** Resources, Writing – review & editing, Supervision, Project administration, Funding acquisition.

Declaration of competing interest

The authors declare that they have no known competing financial interests or personal relationships that could have appeared to influence the work reported in this paper.

Data availability

The source of data has been shared in the article. The data is open source.

Acknowledgments

This study was funded by the Fundamental Research Funds for the Central Universities (2022YJS095). We also acknowledge Ali Moti Nasrabadi for providing the EEG dataset. Both authors have read and agreed to the published version of the manuscript.

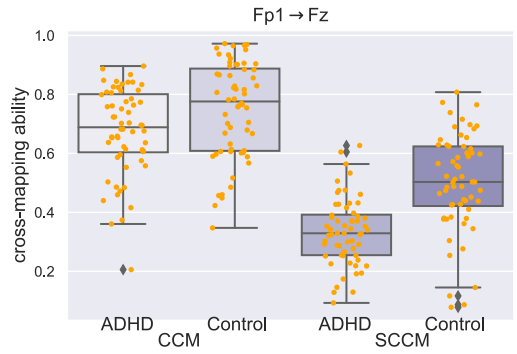

(a)

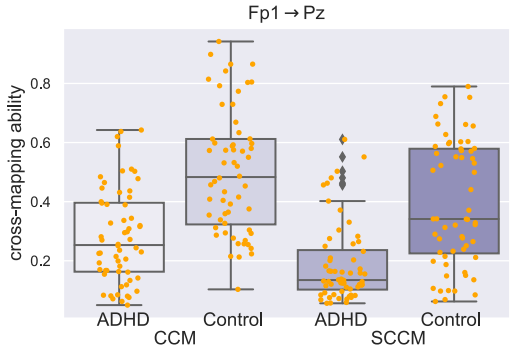

(b)

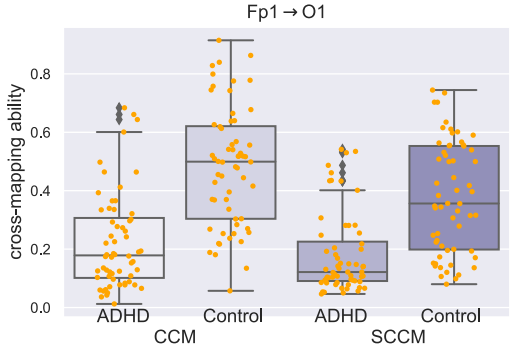

(c)

Fig. 10. The box plots of cross-mapping ability. (a) Fp1→Fz. (b) Fp1→Pz. (c) Fp1→O1.

References

[1] Gettelman Andrew, Geer Alan J, Forbes Richard M, Carmichael Greg R, Feingold Graham, Posselt Derek J, Stephens Graeme L, van den Heever Susan C, Varble Adam C, Zuidema Paquita. The future of Earth system prediction: Advances in model-data fusion. Sci Adv 2022;8(14):eabn3488.

[2] Friston Karl, Moran Rosalyn, Seth Anil K. Analysing connectivity with Granger causality and dynamic causal modelling. Curr Opin Neurobiol 2013;23(2):172–8.

[3] Lin Aijing, Liu Kang KL, Bartsch Ronny P, Ivanov Plamen Ch. Dynamic network interactions among distinct brain rhythms as a hallmark of physiologic state and function. Commun Biol 2020;3(1):1–11.

[4] Pearl Judea. Models, reasoning and inference, Vol. 19. Cambridge, UK: CambridgeUniversityPress; 2000, p. 2.

[5] Granger Clive WJ. Investigating causal relations by econometric models and cross-spectral methods. Econometrica 1969;424–38.

[6] Schreiber Thomas. Measuring information transfer. Phys Rev Lett 2000;85(2):461.

[7] Sugihara George, May Robert, Ye Hao, Hsieh Chih-hao, Deyle Ethan, Fogarty Michael, Munch Stephan. Detecting causality in complex ecosystems. Science 2012;338(6106):496–500.

[8] Runge Jakob, Bathiany Sebastian, Bollt Erik, Camps-Valls Gustau, Coumou Dim, Deyle Ethan, Glymour Clark, Kretschmer Marlene, Mahecha Miguel D, Muñoz-Marí Jordi. Inferring causation from time series in Earth system sciences. Nature Commun 2019;10(1):1–13.

[9] Ye Hao, Deyle Ethan R, Gilarranz Luis J, Sugihara George. Distinguishing time-delayed causal interactions using convergent cross mapping. Sci Rep 2015;5(1):1–9.

[10] Yang Albert C, Peng Chung-Kang, Huang Norden E. Causal decomposition in the mutual causation system. Nature Commun 2018;9(1):1–10.

[11] De Brouwer Edward, Arany Adam, Simm Jaak, Moreau Yves. Latent convergent cross mapping. In: International conference on learning representations.

[12] Wang Yunqian, Yang Jing, Chen Yaning, De Maeyer Philippe, Li Zhi, Duan Weili. Detecting the causal effect of soil moisture on precipitation using convergent cross mapping. Sci Rep 2018;8(1):1–8.

[13] Schiecke Karin, Pester Britta, Feucht Martha, Leistritz Lutz, Witte Herbert. Convergent cross mapping: Basic concept, influence of estimation parameters and practical application. In: 2015 37th annual international conference of the IEEE engineering in medicine and biology society. EMBC, IEEE; p. 7418–21.

[14] Guo Zhen, Hao Mengyan, Yu Bin, Yao Baozhen. Detecting delay propagation in regional air transport systems using convergent cross mapping and complex network theory. Transp Res E 2022;157:102585.

[15] Ge Xinlei, Lin Aijing. Kernel change point detection based on convergent cross mapping. Commun Nonlinear Sci Numer Simul 2022;109:106318.

[16] Mønster Dan, Fusaroli Riccardo, Tylén Kristian, Roepstorff Andreas, Sherson Jacob F. Causal inference from noisy time-series data—testing the convergent cross-mapping algorithm in the presence of noise and external influence. Future Gener Comput Syst 2017;73:52–62.

[17] Feng Guanchao, Yu Kezi, Wang Yunlong, Yuan Yilian, Djurić Petar M. Improving convergent cross mapping for causal discovery with Gaussian processes. In: ICASSP 2020-2020 IEEE international conference on acoustics, speech and signal processing. ICASSP, IEEE; p. 3692–6.

[18] Stavroglou Stavros K, Pantelous Athanasios A, Stanley H Eugene, Zuev Konstantin M. Hidden interactions in financial markets. Proc Natl Acad Sci 2019;116(22):10646–51.

[19] Stavroglou Stavros K, Pantelous Athanasios A, Stanley H Eugene, Zuev Konstantin M. Unveiling causal interactions in complex systems. Proc Natl Acad Sci 2020;117(14):7599–605.

[20] Bandt Christoph, Pompe Bernd. Permutation entropy: a natural complexity measure for time series. Phys Rev Lett 2002;88(17):174102.

[21] Staniek Matthäus, Lehnertz Klaus. Symbolic transfer entropy. Phys Rev Lett 2008;100(15):158101.

[22] Ouyang Gaoxiang, Dang Chuangyin, Richards Douglas A, Li Xiaoli. Ordinal pattern based similarity analysis for EEG recordings. Clin Neurophysiol 2010;121(5):694–703.

[23] Parlitz Ulrich, Berg Sebastian, Luther Stefan, Schirdewan Alexander, Kurths Jürgen, Wessel Niels. Classifying cardiac biosignals using ordinal pattern statistics and symbolic dynamics. Comput Biol Med 2012;42(3):319–27.

[24] Zanin Massimiliano, Olivares Felipe. Ordinal patterns-based methodologies for distinguishing chaos from noise in discrete time series. Commun Phys 2021;4(1):1–14.

[25] Steuer Ralf, Kurths Jürgen, Daub Carsten O, Weise Janko, Selbig Joachim. The mutual information: detecting and evaluating dependencies between variables. Bioinformatics 2002;18(2):S231–40.

[26] Yin Yi, Wang Xi, Li Qiang, Shang Pengjian, Gao He, Ma Yan. Multiscale permutation mutual information quantify the information interaction for traffic time series. Nonlinear Dynam 2020;102(3):1909–23.

[27] Vinh Nguyen Xuan, Epps Julien, Bailey James. Information theoretic measures for clusterings comparison: is a correction for chance necessary? In: Proceedings of the 26th annual international conference on machine learning. p. 1073–80.

[28] Darbellay Georges A, Vajda Igor. Estimation of the information by an adaptive partitioning of the observation space. IEEE Trans Inform Theory 1999;45(4):1315–21.

[29] Johnson Jay R, Wing Simon. A solar cycle dependence of nonlinearity in magnetospheric activity. J Geophys Res Space Phys 2005;110(A4).

[30] Schiff Steven J, So Paul, Chang Taeun, Burke Robert E, Sauer Tim. Detecting dynamical interdependence and generalized synchrony through mutual prediction in a neural ensemble. Phys Rev E 1996;54(6):6708.

[31] Motie Nasrabadi Ali, Allahverdy Armin, Samavati Mehdi, Mohammadi Mohammad Reza. EEG data for ADHD / control children. 2020.

[32] Ekhlasi Ali, Nasrabadi Ali Motie, Mohammadi Mohammad Reza. Direction of information flow between brain regions in ADHD and healthy children based on EEG by using directed phase transfer entropy. Cogn Neurodyn 2021;15(6):975–86.

[33] Xia Mingrui, Wang Jinhui, He Yong. BrainNet Viewer: a network visualization tool for human brain connectomics. PLoS One 2013;8(7):e68910.